Front. Phys., 2012, 7(5): 527–532
DOI 10.1007/s11467-012-0252-1

RESEARCH ARTICLE

Steady-state property and dynamics in graphene-nanoribbon-array lasers

Xing-Hai Zhao[1,*], **Guang-Cun Shan**[2,†], **Chan-Hung Shek**[2]

[1] *Institute of Electronic Engineering, China Academy of Engineering Physics, Mianyang 621900, China*
[2] *Department of Physics and Materials Science, City University of Hong Kong, Hong Kong SAR, China*

*E-mail: *xinghai839@yahoo.cn, †041055004@fudan.edu.cn*
Received December 22, 2011; accepted March 21, 2012

In this work, we present a schematic configuration and device model for a graphene-nanoribbon (GNR)-array-based nanolaser, which consists of a three-variable rate equations that takes into account carrier capture and Pauli blocking in semiconductor GNR-array lasers to analyze the steady-state properties and dynamics in terms of the role of the capture rate and the gain coefficient in GNR array nanolasers. Furthermore, our GNR-array nanolaser device model can be determined as two distinct two-variable reductions of the rate equations in the limit of large capture rates, depending on their relative values. The first case leads to the rate equations for quantum well lasers, exhibiting relaxation oscillations dynamics. The second case corresponds to GNRs nearly saturated by the carriers and is characterized by the absence of relaxation oscillations. Our results here demonstrated that GNR-array as gain material embedded into a high finesse microcavity can serve as an ultralow lasing threshold nanolaser with promising applications ranging widely from optical fiber communication with increasing data processing speed to digital optical recording and biology spectroscopy.

Keywords graphene nanoribbon, graphene nanoribbon laser, laser theory, laser model

PACS numbers 42.55.Ah, 42.55.Px, 42.60.Rn, 78.67.Hc, 78.67.Wj

1 Introduction

After more than two decades of rapid development, semiconductor lasers are now being used in a wide range of important applications including optical fiber communication, digital optical recording, laser materials processing, biology and medicine, imaging, spectroscopy, etc. However, they suffer from limitations such as relatively high threshold powers, multi-mode operation, problems with direct modulation above 10 GHz, and difficulty in growing their distributed Bragg reflectors for long-haul communications wavelengths. In view of the fact that the quantum size effects leading to an increase in the density of states near the band edges can lower the lasing threshold and achieve a spectral tuning ability without changing chemical composition, quantum dots (QDs) were introduced in the 1990s as an alternative to quantum wells (QWs). The possibility of realizing a semiconductor QD laser in which the threshold is ultimately minimized (the so-called thresholdless laser) by eliminating spontaneous emission as far as possible is attracting considerable attention. Since 1997, the response of QD lasers have been systematically investigated through relaxation oscillation (RO) measurements [1–5], the result showing stronger damping than conventional QW lasers. QD edge-emitting lasers at 1300 nm on GaAs substrates out-perform InP-based QW edge-emitters in several important aspects such as threshold current, temperature stability, chirp, and feedback insensitivity [1, 2]. However, the feasibility of high-speed transmission rates strongly depends on the damping rate of the ROs which inevitably appear in gain-switched operations [3]. Most of the research work on low dimensional nanostructures has first been focused on QWs due to the lack of reliable methods for fabricating sufficiently high-quality QDs at that time.

On the other hand, since the successful fabrication and measurement of graphene [6], extensive interesting research efforts on graphene layer structures and graphene nanoribbons (GNRs) have been devoted to exploring their promising applications [6–12]. In this regard, re-

cent advances in fabricating and characterizing stable GNRs have paved the way to functioning as one of the building blocks for nanoscale optoelectronic and photonic devices and circuits [7–11]. Moreover, depending on specific GNRs, theoretical studies using tight binding or massless Dirac fermion equation approaches have predicted GNRs to be either metals or semiconductors [12, 13], whereas density functional theory (DFT) calculations showed that all armchair-edged GNRs (AGNRs) are semiconducting with an energy gap scaling with the inverse of the GNR width [14]. In particular, first-principle many-electron Green's function approach studies within the GW approximation [14, 15] have shown that AGNRs should have an energy spectrum consisting of a series of discrete lines due to the low-dimensional confinement of the many-body electron–hole states. The quasi-particle band gap of AGNRs is in the interesting energy range of 1–3 eV for 2–1 nm wide GNRs due to many-electron effects, and they may find applications in low cost nanolasers and transmitter modules by releasing the need for temperature control, isolators, and external modulators. These recent advances in GNRs, in connection with several intensive theoretical studies to investigate the RO frequency and damping rate of QW lasers, can guide the theoretical model study and provide guideline for realizing a practical GNR-array nanolaser.

In this work, we present a three-variable rate equation model based on the modified two-variable QW rate Eqs. [16] in a form suitable for GNR-array nanolasers to understand the origin of novel properties of our designated GNR-array nanolasers. Since so far their precise values are difficult to determine experimentally, our aim here is to derive useful analytical equations and present meaningful numerical results, from which we can get important clues and discuss some novel properties of the GNR-array nanolasers for possible range of values of several parameters. Besides, due to the multiple time scales of the GNR laser, we find that two markedly different dynamical laser responses are possible depending on their specific designs.

2 Models

As illustrated in Fig. 1, we consider an array of AGNRs, which are first grown on insulating silicon carbide (SiC) surfaces by high temperature annealing in vacuum, and then lithographically embedded in a high Fabry–Perot cavity device. It is important to recognize that GNRs with a lateral size distribution work perfectly well for this lateral carrier confinement. The two-dimensional confinement in GNRs provides the desired lateral carrier confinement. The as-fabricated GNR size variation achieved so far can be sufficiently small to provide enough gain for lasing at lower GNR states. In such a semiconductor GNR-array laser device, the carriers are first injected into an SiC layer before being captured by a GNR. In addition to the electrical field in the cavity and the carrier density in the insulating layer, we need to introduce the occupation probability of a GNR and consider three rate equations that take into account the carrier capture process and Pauli blocking [2–4]. Integrating this two-stage process and the atom-like quantum emitter characteristics of GNRs similar to QDs, the rate equations for our semiconductor GNR-array-based devices can be modeled by means of the QD-based laser rate equations formulated by O'Brien *et al.* [3] and Uskov *et al.* [4] and further developed by Erneux *et al.* [5]. The model analysis method here closely follows that of Refs. [4, 5]. Besides, it is worth pointing out that our GNR nanolaser proposed here can be implemented by such an electrically pumped GNRs embedded into a high Fabry–Perot cavity, which is more robust to act as a nanophotonic device and can be readily integrated for future all-graphene-based monolithic optoelectronic integrated circuits (MOEICs).

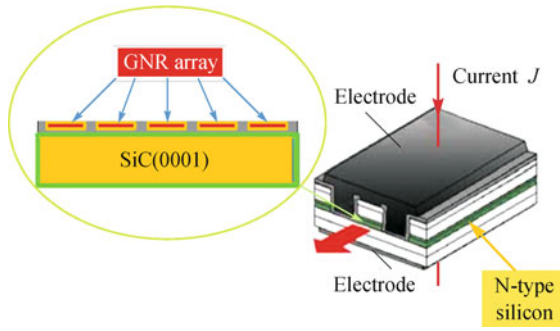

Fig. 1 Schematic illustration of the AGNR-array laser device.

Without the loss of generality, the dynamics of a GNR-array nanolaser is modeled by a set of three coupled rate equations for the electric field E in the cavity, the number of carriers in the insulating layer per GNR, N, and the occupation probability of a GNR in the laser pumped with the current per GNR J. In terms of the intensity $I = E^2$, these equations are

$$\frac{\mathrm{d}I}{\mathrm{d}t} = -\gamma_s I + v_g g_0 (2\rho - 1) I \tag{1}$$

$$\frac{\mathrm{d}\rho}{\mathrm{d}t} = -\gamma_d \rho + CN(1-\rho) - v_g \sigma_s (2\rho - 1) \tag{2}$$

$$\frac{\mathrm{d}N}{\mathrm{d}t} = -\gamma_n N + J/q - 2CN(1-\rho) \tag{3}$$

The last term $CN(1-\rho)$ in Eq. (3) describes the rate of capture, which is proportional to the number of carriers present as well as the probability to find a GNR. The factor 2 in Eq. (3) accounts for the twofold spin degeneracy in the GNR energy levels. A similar factor 2 is also included in the definition of the differential gain factor g in Eq. (1) [3–5]. The parameters γ_n and γ_d represent non-radiative decay rates, v_g is the group velocity and σ_s is the cross section of interaction of the carriers in a

GNR with the electrical field. γ_s is the photon decay rate in the cavity and g_0 is the differential gain. Introducing the dimensionless variables

$$\tau = \gamma_s t, \quad n = N, \quad \text{and} \quad I_1 = \gamma_d^{-1} v_g \sigma I \tag{4}$$

into Eqs. (1)–(3), we obtain

$$\frac{\mathrm{d}I_1}{\mathrm{d}\tau} = [-1 + g\,(2\rho - 1)]I_1 \tag{5}$$

$$\frac{\mathrm{d}\rho}{\mathrm{d}\tau} = \eta_{ds}\left[-\rho + Bn\,(1-\rho) - (2\rho - 1)\,I_1\right] \tag{6}$$

$$\frac{\mathrm{d}n}{\mathrm{d}\tau} = \eta_{ns}\left[-n + J_1 - 2Bn\,(1-\rho)\right] \tag{7}$$

where $\eta_{ds} = \gamma_d/\gamma_s$, $\eta_{ns} = \gamma_n/\gamma_s$, $g = \gamma_s^{-1} v_g g_0$, $J_1 = \gamma_n^{-1} J/q$, and $B = \gamma_d^{-1} C$. Note that the last term in Eq. (7) is usually denoted with $F(\rho,\ n) = Bn(1-\rho)$. With $\gamma_d = 10^{-3}$ ps^{-1} [9, 11] and the realistic values of the physical parameters reported both theoretically and experimentally so far [9–15], we determine $g = 1.25 - 5.0$, $B = 10 - 500$, and $\eta = 10^{-3}$ for GNRs. Note that larger values of B are possible since values of the capture time C^{-1} from 1 to 10^2 ps have been reported in the literature. The rate equations formulated by O'Brien *et al.* [3] consist of three equations for the intensity I of the laser field in the cavity, the occupation probability of a GNR in the laser, and the number n of carriers in the insulating layer per GNR. The parameter $\eta = 10^{-3}$ is the ratio between the carrier and photon decay rates. Note that the relaxation rates of ρ and n are assumed equal for mathematical simplicity. J is the pump current per GNR and is the control parameter. The function $F(\rho,\ n)$ describes the carrier exchange rate between the insulating layer and the GNRs. In general, the carrier exchange rate can be formulated as [5]

$$F(\rho,\ n) = R^{\mathrm{cap}}(1-\rho) - R^{\mathrm{esc}} \tag{8}$$

where $1-\rho$ is the Pauli blocking factor, $R^{\mathrm{cap}} = Bn$ describes the carrier capture with a rate $B \sim 10^2$, and R^{esc} describes the carrier escape from the GNRs to the insulating layer. At room temperature, $R^{\mathrm{cap}} \gg R^{\mathrm{esc}}$ and we shall ignore the escape process by assuming $R^{\mathrm{esc}} = 0$ reasonably. The three parameters B, η and $g-1$ control the time-dependent response of the GNRs laser. Since their precise values are difficult to evaluate experimentally, our objective is to derive meaningful analytical equations and present meaningful results valid for possible range of values of B, g, and η.

3 Equations and results

In the following sections, we solve Eqs. (1)–(3) using η as our order parameter to determine the steady-states, and also dynamics, for it does not appear in the expressions of the steady-states. Apart from the zero intensity solution, there exists a nonzero intensity steady-state given by

$$\rho_{ss} = \frac{1}{2}\left(1 + g^{-1}\right) \tag{9}$$

$$n_{ss} = \frac{J}{1 + B\,(1 - g^{-1})} = \frac{J}{1 + B_e} \tag{10}$$

$$\begin{aligned} I_{ss} &= \frac{g}{2}\frac{B\left(1-g^{-1}\right)}{1 + B\,(1-g^{-1})} \\ &\quad \cdot \left[J - \frac{1 + B\left(1-g^{-1}\right)}{B\,(1-g^{-1})}\left(1+g^{-1}\right)\right] \\ &= \frac{g}{2}\frac{B_e}{1+B_e}\,(J - J_{th}) \end{aligned} \tag{11}$$

where $B_e = B(1-g^{-1})$ and $J_{th} = \frac{1+B_e}{B_e}\left(1+g^{-1}\right)$ are defined as the effective capture rate and the laser threshold pump current per GNR, respectively. Figures 2(a) and (b) illustrate the steady-state property as a function of J for different values of the capture rate B as well as the effect of gain parameter g. It is apparent that the steady-state intensity I_{ss} increases with increasing g values. More importantly, it is found that the threshold becomes smaller with increasing g values. This property is indeed novel and should be observable in future practical GNR nanolaser devices. Compared to Fig. 2(b), where $B = 50$, Fig. 2 (a), where $B = 200$, exhibits larger steady-state intensity I_{ss}. We note from Eq. (9) that the steady-state occupation probability is close to 1, meaning the GNR saturation. As a consequence, the carriers cannot be captured by GNRs and their number will be controlled only by the field in the cavity.

Then, following the linearization analysis method in Ref. [5], we obtain the linearized equations to formulate the characteristic equation for the growth rate σ using the steady-state intensity I_{ss} as the control parameter instead of J for convenience mathematically. This characteristic equation is

$$\sigma^3 + a_1\sigma^2 + a_2\sigma + a_3 = 0 \tag{12}$$

where

$$a_1 = \eta\left[1 + B_e + \frac{2\,(1+I_{ss})}{1-g^{-1}}\right] \tag{13}$$

$$a_2 = \eta\left[2I_{ss} + \eta\frac{2\,(1+I_{ss})}{1-g^{-1}} + \eta B_e\,(1+2I_{ss})\right] \tag{14}$$

$$a_3 = 2I_{ss}\eta^2\,(1+B_e) \tag{15}$$

At this step, a linear stability analysis can be performed about the steady-state lasing fixed point of Eq. (12) to understand how the system reacts to perturbations. Using the Routh–Hurwitz conditions [18], we find that the steady-state is always stable. Moreover, following the method in Ref. [5], we introduce

$$\sigma = \eta^{1/2}\lambda_0 + \eta\lambda_1 + \cdots \tag{16}$$

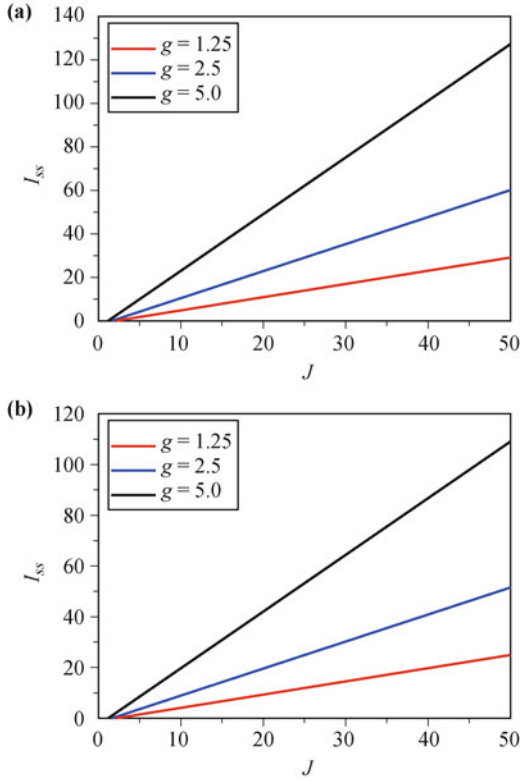

Fig. 2 Steady-state property as a function of J. $B = 200$ **(a)** and 50 **(b)**, and $g = 1.25$ (*red line*), 2.5 (*green line*) and 5.0 (*black line*).

into Eq. (13) and equate to zero the coefficients of each power of $\eta^{1/2}$. This leads to a series of linear problems for $\lambda_0, \lambda_1, \cdots$. As a result, we obtain

$$\sigma_{1,2} \approx \pm \mathrm{i} \left(2\eta I_{ss}\right)^{1/2} - \eta \frac{1 + I_{ss}}{1 - g^{-1}} \tag{17}$$

$$\sigma_3 \approx -\eta \left(1 + B_e\right) \tag{18}$$

At this point, it is found that the real part of Eq. (17) gives the damping rate

$$\Gamma_d = \eta \frac{1 + I_{ss}}{1 - g^{-1}} \tag{19}$$

It is concluded here that Eq. (19) suggests that B does not have a strong effect since it appears only through I_{ss}, given by Eq. (10), which remains $O(1)$ as $B \to \infty$. And the imaginary part of Eq. (17) gives the RO frequency

$$\Omega_{RO} = \left(2\eta I_{ss}\right)^{1/2} \tag{20}$$

which is identical with the RO frequency of QW lasers.

Furthermore, by introducing $\sigma = \eta^{1/2}\lambda$ into Eq. (9), the equation for λ is then given by

$$\lambda^3 + b_1\lambda^2 + b_2\lambda + b_3 = 0 \tag{21}$$

where

$$b_1 = \eta^{1/2} \left[1 + B_e + \frac{2\left(1 + I_{ss}\right)}{1 - g^{-1}}\right] \tag{22}$$

$$b_2 = 2I_{ss} + \eta^{1/2} \frac{2\left(1 + I_{ss}\right)}{1 - g^{-1}} + \eta B_e \left(1 + 2I_{ss}\right) \tag{23}$$

$$b_3 = 2I_{ss}\eta^{1/2} \left(1 + B_e\right) \tag{24}$$

To investigate the effect of large capture rate B, following the method in Ref. [5]. We expand $I = I\left(B_e^{-1}\right)$ as a function of B_e^{-1}, and by introducing

$$B_e = \eta^{-1/2} B_1 \tag{25}$$

into Eq. (22) in seeking a solution of the form

$$\lambda = \lambda_0 + \eta^{1/2}\lambda_1 + \cdots \tag{26}$$

we obtain a series of new problems for $\lambda_0, \lambda_1, \cdots$. The leading problem for λ_0 is

$$\lambda_0^3 + B_1\lambda_0^2 + 2I_0\lambda_0 + 2I_0B_1 = 0 \tag{27}$$

which gives the solutions

$$\lambda_{01,02} = \pm \mathrm{i} \left(2I_0\right)^{1/2} \tag{28}$$

$$\lambda_{03} = -B_1 \tag{29}$$

The expression of the RO frequency provided by Eq. (28) is identical with Eq. (20) with $I_{ss} = I_0$. To determine the RO damping rate, we investigate the next order problem for λ_1 following the method in Ref. [5], and then we obtain

$$\mathrm{Re}\left(\lambda_1\right) = \frac{-1}{\left(2I_0 + B_1^2\right)} \left[\frac{2\left(1 + I_0\right)}{1 - g^{-1}} I_0 + \frac{B_1^2}{2}\left(1 + 2I_0\right)\right] \tag{30}$$

Note that $\mathrm{Re}\left(\lambda_1\right) \to -\Gamma_1/\eta$ as $B_1 \to 0$, where Γ_1 is defined by Eq. (17). The damping rate of the GNR nanolaser vs. the capture rate B is shown in Fig. 3. The damping rate decreases in the limit of very large B, but it should also be noted from the first term in the right-hand side of Eq. (30) that a value g close to 1 will contribute to an increase of the damping rate.

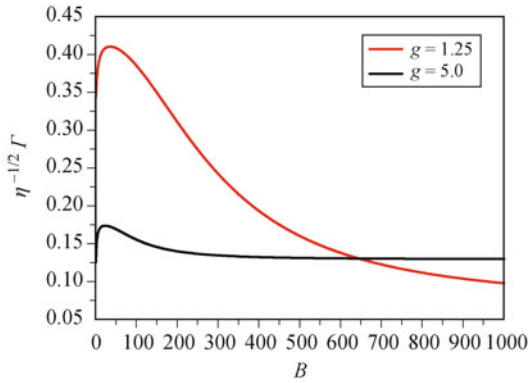

Fig. 3 Damping rate as a function of B. $J - J_{th} = 1$, $\eta = 10^{-3}$, and $g = 1.25$ (*red line*) and 5.0 (*black line*).

In fact, the capture rate of the carriers into empty GNRs contributes to the damping of the relaxation oscillations. In the limit of large effective capture rates, i.e., $B_e = B(1 - g^{-1}) \to \infty$, the RO damping rate Γ decreases and approaches the value Γ_{QW} of the QW laser. This may be understood as follows. If the capture rate is too large, the number of available carriers n will be small and the

GNR laser will behave like a conventional laser. On the other hand, we have shown that the GNR damping rate is larger than the QW damping rate if $B_e = O(1)$. This can be realized even for large capture rates B provided that the deviation $g-1$ is as small as B^{-1}.

To deeply understand the combined effects of large B and small $g-1$, we consider the large B limit of the full rate Eqs. (1)–(3) and derive two distinct limits depending on g. As we shall solve them using the 4–5th Ruter–Kuttger method and demonstrate, these two limits lead to the equations for a class B laser and a class A laser, respectively [16, 17].

The first case is defined by the scaling $B = O(\eta^{-1/2})$ and $g-1$ being arbitrary and fixed. By introducing $n = B\bar{n}$ into Eqs. (1)–(3), we note from Eq. (3) that $\bar{n}$ can be eliminated adiabatically as

$$\bar{n} = \frac{J}{2(1-\rho)} \tag{31}$$

The remaining equations for the gain $G = g(2\rho-1)$ and I then become

$$\frac{\mathrm{d}I}{\mathrm{d}t} = (-1+G)I \tag{32}$$

$$\frac{\mathrm{d}G}{\mathrm{d}t} = \eta[J-g-G(1+2I)] \tag{33}$$

which are essentially the rate equations for QW laser. This case corresponds to the rate equations for QW lasers, exhibiting RO dynamics significantly as demonstrated in Fig. 4(a).

The second case is defined by the scaling $B = O(\eta^{-1})$ and $g-1 = O(h)$ taking the scaling relations of $1-g^{-1} = \eta d$ and $B = \eta^{-1}B_1$, as suggested by the analysis in Ref. [5]. In addition, we introduce the new time $s = \eta t$ into Eqs. (1)–(3), and also a new quantity $\bar{\rho} = \frac{1+I}{B_1 n}$ that can be eliminated adiabatically to obtain the remaining equations for I and n

$$\frac{\mathrm{d}I}{\mathrm{d}s} = \left(d - 2\frac{1+I}{B_1 n}\right) I \tag{34}$$

$$\frac{\mathrm{d}n}{\mathrm{d}s} = J - n - 2(1+I) \tag{35}$$

where the differentiation is done with respect to the time variable s. In this limit, the decay of the ROs occurs on the same time scale as the dynamics of ROs, as demonstrated in Fig. 4(c). This case corresponds to GNRs nearly saturated by the carriers and is apparently characterized by the absence of relaxation oscillations.

As demonstrated above, the first case is characterized by the decay rate of the carriers which is much smaller than the decay rate of the photons in the cavity, whereas the second case is characterized by comparable time scales for both the photons and carriers. Figures 4(b) and (d) compare the dynamics in the phase space

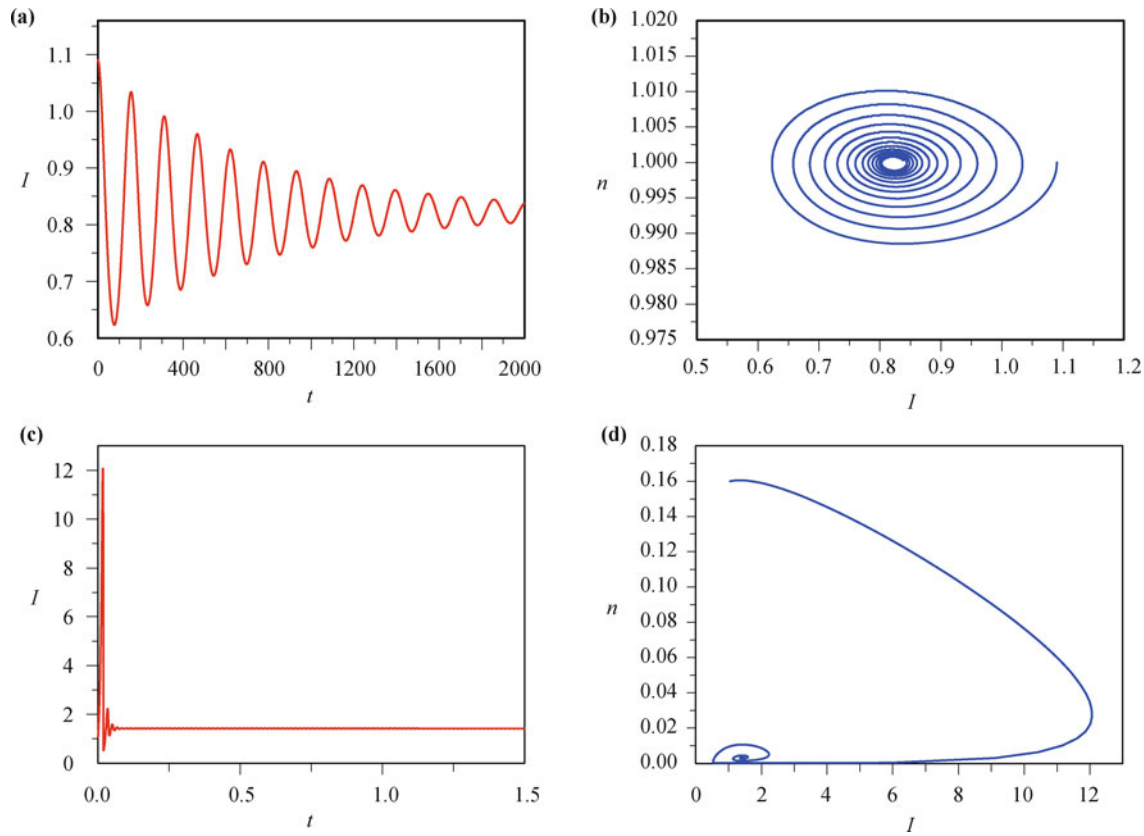

Fig. 4 Solution of the two-variable limits of three-variable rate equations for GNR-array nanolaser. **(a)**, **(b)** Solution of Eqs. (32) and (33) with $I(t=0) = I_{ss} + 0.1$ and $G(0) = G_{ss} = 1$. **(c)**, **(d)** Solution of Eqs. (34) and (35) with $I(t=0) = I_{ss} + 0.1$ and $n(0) = n_{ss} = 0.15$. The values of the fixed parameters are $g = 1.25$, $B = 10^3$, and $h = 10^{-3}$. All variables are dimensionless. Time is normalized by the photon lifetime.

for the two limiting cases. The fixed parameters are identical and the perturbation of the steady-state initiating the oscillatory decay is the same. The excellent performance of GNR-array-based nanolaser is attributed to the unique electronic structures and excitonic properties of GNRs [6–12], which is different from QDs. Besides, the utilization of such a GNR-array-based nanolaser device can be extended for the achievement of lasing with the frequencies of about 1 THz at room temperature due to the higher efficiency of electrical pumping, as compared to the optically pumped multilayer-graphene structures [19]. A more complicated microscopically based rate equation model for GNR lasers is under study, which separately treats the dynamics of electrons and holes, and the carrier–carrier scattering rates, depending nonlinearly on the insulating layer carrier densities.

4 Conclusions

We have presented a novel schematic configuration and device model for a GNR-array-based nanolaser in terms of rate equations to analyze the steady-state properties and dynamics in terms of the role of the capture rate and the gain coefficient in GNR array nanolasers. Our analysis is based on a linearized theory proposed by Erneux *et al.* [5] without anticipating the nonlinear response of the laser perturbation. Our results here demonstrated that, as gain material embedded into a high finesse microcavity functioning as a nanolaser device, GNR-array can be determined to be two distinct two-variable reductions of the rate equations in the limit of large capture rates, depending on their relative values of the capture rate and the gain coefficient. Although there have been no GNR-array-based nanolaser device available so far, the rate equation model and the results discussed here are expected to serve as a versatile and useful guideline for future studies of GNR-array-based nanolaser. Such GNR nanolaser devices are promising for important applications in optical fiber communication with increasing data processing speed, digital optical recording, biology and medicine imaging, and some others. Our work here provides the theoretical foundation and guideline for the developments of the monolithic integration of GNR-based nanophotonic integrated circuits with graphene-based CMOS.

Acknowledgements This work was supported by the Key Program of Science and Technology Development Foundation, China Academy of Engineering Physics (Grant No. 2008A0403016), and the Strategic Research Grant (Grant No. 7008101) from City University of Hong Kong.

References

1. D. Bimberg, M. Grundmann, and N. N. Ledentsov, Quantum Dot Heterostructures, New York: Wiley, 1999
2. M. Kuntz, N. N. Ledentsov, D. Bimberg, A. R. Kovsh, V. M. Ustinov, A. E. Zhukov, and Y. M. Shernyakov, Appl. Phys. Lett., 2002, 81(20): 3846
3. D. O'Brien, S. P. Hegarty, G. Huyet, and A. V. Uskov, Opt. Lett., 2004, 29: 1074
4. S. Melnik, G. Huyet, and A. V. Uskov, Opt. Express, 2006, 14(7): 2950
5. T. Erneux, E. A. Viktorov, and P. Mandel, Phys. Rev. A, 2007, 76(2): 023819
6. K. S. Novoselov, A. K. Geim, S. V. Morozov, D. Jiang, Y. Zhang, S. V. Dubonos, I. V. Grigorieva, and A. A. Firsov, Science, 2004, 306(5696): 666
7. K. V. Emtsev, A. Bostwick, K. Horn, J. Jobst, G. L. Kellogg, L. Ley, J. L. McChesney, T. Ohta, S. A. Reshanov, J. Röhrl, E. Rotenberg, A. K. Schmid, D. Waldmann, H. B. Weber, and T. Seyller, Nat. Mater., 2009, 8(3): 203
8. C. Stampfer, S. Fringes, J. Guttinger, F. Molitor, C. Volk, B. Terres, J. Dauber, S. Engels, S. Schnez, A. Jacobsen, S. Droscher, T. Ihn, and K. Ensslin, Front. Phys., 2011, 6(3): 271
9. Z. Chen, Y. M. Lin, M. J. Rooks, and P. Avouris, Physica E, 2007, 40(2): 228
10. M. Y. Han, B. Özyilmaz, Y. Zhang, and P. Kim, Phys. Rev. Lett., 2007, 98(20): 206805
11. F. Bonaccorso, Z. Sun, T. Hasan, and A. C. Ferrari, Nat. Photon., 2010, 4(9): 611
12. G. C. Shan, X. H. Zhao, and W. Huang, J. Nanoelectron. Optoelectron., 2011, 6(2): 138
13. L. Brey and H. A. Fertig, Phys. Rev. B, 2006, 73(23): 235411
14. L. Yang, C. H. Park, Y. W. Son, M. L. Cohen, and S. G. Louie, Phys. Rev. Lett., 2007, 99(18): 186801
15. L. Yang, M. L. Cohen, and S. G. Louie, Nano Lett., 2007, 7(10): 3112
16. J. R. Tredicce, F. T. Arecchi, G. L. Lippi, and G. P. Puccioni, J. Opt. Soc. Am. B, 1985, 2(1): 173
17. A. Fiore and A. Markus, IEEE J. Quantum Electron., 2007, 43(4): 287
18. J. V. Uspensky, Theory of Equations, New York: McGraw-Hill, 1948
19. V. Ryzhii, M. Ryzhii, A. Satou, T. Otsuji, A. A. Dubinov, and V. Ya. Aleshkin, J. Appl. Phys., 2009, 106(8): 084507